Substrate and Finite-Thickness-Induced Uncertainties in Surface Impedance Measurements of Thin Conducting Films

Nicola Pompeo, *Senior Member, IEEE*, Andrea Alimenti, *Member, IEEE*, Kostiantyn Torokhtii, *Member, IEEE*, Pablo Vidal García, *Member, IEEE*, and Enrico Silva, *Senior Member, IEEE*

***Abstract*— Measurements of the surface impedance of conducting, semiconducting, and superconducting materials are commonly used in research, metrology, and industry to extract and study the resistivity of the material. The interest is often devoted to thin films because of: 1) the possibility to grow nearly perfect materials, essential for research; 2) ease of reproducibility for metrological standards; or 3) direct applications in the electronic industry. However, in finite-thickness films, the probing electromagnetic (e.m.) field leaks through the film to the underlying substrate. The substrate then gives a substantial contribution to the measured surface impedance and, thus, to the extracted resistivity. While the e.m. problem is well known, analyses in terms of the evaluation of the uncertainty involved are scarce. Moreover, simplified models for the measured surface impedance with different ranges of applicability are often used in order to simplify the analysis or to highlight the main physics. Also, in these cases, these approaches are seldom followed by careful evaluation of the additional uncertainty so introduced. In this article, we thoroughly study when simplified models, which neglect the substrate contribution, can be used, and we identify the situations in which the substrate properties yield negligible contributions to the extracted resistivity and its uncertainty. To do so, we discuss the various sources of uncertainty, also with the help of a brief description of typical measurement techniques. We show that the simplified models can greatly simplify the extraction of the material resistivity from the measured surface impedance, with reduced uncertainty and also reduced computational cost for its evaluation. We find that ranges in frequency and film thickness exist, where the simplified models can be used, with negligible approximation errors, once compared with the uncertainties related to the measurement technique. However, the identification of such combined ranges is not trivial, being particularly critical for superconducting films. Finally, we report experimental measurements of the surface impedance of different superconducting samples (bulks and the more critical situation of films over layered structures), providing case studies for both the determination of the uncertainties and the validation of the models.**

***Index Terms*— Microwave measurements, superconducting materials, surface impedance, thin films, uncertainty.**

Received 1 July 2024; accepted 12 September 2024. Date of publication 2 December 2024; date of current version 12 December 2024. This work was partially supported by the European Organization for Nuclear Research (CERN) Funding through the Addendum FCC-GOV-CC-0218 (KE5084/ATS) within the Future Circular Collider (FCC) study. The Associate Editor coordinating the review process was Dr. Tae-Weon Kang. *(Corresponding author: Nicola Pompeo.)*

The authors are with the Dipartimento di Ingegneria Industriale, Elettronica e Meccanica, Università Roma Tre, 00146 Rome, Italy (e-mail: nicola.pompeo@uniroma3.it).

Digital Object Identifier 10.1109/TIM.2024.3509590

NOMENCLATURE

i	Imaginary unit, $=\sqrt{-1}$.
Z_s	Surface impedance.
Z_{intr}	Intrinsic impedance.
Z_{bulk}	(Super)conductor bulk surface impedance.
Z_{eff}	Effective surface impedance.
Z_{si}	Intrinsic film impedance.
Z_{sf}	Thin film impedance.
$Z_{s[\text{sub}]}$	Generic substrate surface impedance.
Z_m	Bulk metal substrate surface impedance.
Z_d	Infinite thick dielectric substrate surface impedance.
$R\_$ and $X\_$	Resistance and reactance; subscripts as above.
ρ and ρ_{Cu}	Resistivity and room temperature Cu resistivity.
σ	Conductivity, $=1/\rho$.
ε and ε_0	Permittivity and permittivity of vacuum.
ε_r and $\tilde{\varepsilon}$	Relative permittivity and effective complex permittivity.
$\tan\delta_\varepsilon$	Dielectric loss tangent, $=\text{Im}(\varepsilon_r)/\text{Re}(\varepsilon_r)$.
μ and μ_0	Magnetic permeability and magnetic permeability of vacuum.
ν and ω	Frequency and angular frequency $\omega=2\pi\nu$.
$e^{\text{i}\omega\text{t}}$	Complex sinusoid for the sinusoidal regime.
l	Mean free path.
ξ_0	Superconductor coherence length.
λ	London penetration depth.
δ	Penetration depth.
t_s and t_d	Thickness of (super)conductor film | dielectric substrate.
k_s and k_d	Propagation constant in the (super)conductor | dielectric.
ρ_n	Normal state resistivity of a superconductor.
R_n	Normal state surface resistance of a superconductor.
T_c	Critical temperature of a superconductor.
Q, ν_0	Quality factor and resonance frequency of a resonator.
Γ	Reflection coefficient.
S_{ij}	Scattering coefficients of a two-port resonator.
$\Delta\rho_a$, $\Delta\rho_{a\%}$	Normalized approximation error in the simplified model for ρ.
$\Delta Z_{a\%}$	Normalized deviations on Z_s by the simplified model.

I. Introduction

MICROWAVE measurements of the surface impedance are often used to characterize and study conductive materials [1], including the cases of semiconductors [2] and superconductors [3]. The goal is to extract the material complex resistivity ρ from the measurements. The surface impedance is defined as the ratio of the tangential components of the impinging electric and magnetic fields on the material surface, $Z_s = E_t/H_t$. For conducting and superconducting materials, in the local limit, the surface impedance of bulk specimens, i.e., having thickness much larger than the electromagnetic (e.m.) field penetration depth (see Section II), is straightforwardly related to the material resistivity ρ only. On the other hand, measurements often concern thin films because of the possibility of growing nearly perfect materials and single-crystalline samples essential for research and selected applications [4], [5], [6], for the ease of reproducibility for, e.g., metrological standards [7], or for direct applications of thin films in the electronic industry. However, in finite-thickness films, the probing e.m. field reaches the underlying substrate, which contributes to shaping the overall e.m. response of the layered structure. The resulting *effective* surface impedance Z_{eff} is then determined by both the film and the substrate. Since the substrate properties are often known with poor accuracy, the uncertainty on the extracted ρ from the measured Z_s is potentially large. It is, thus, desirable to check whether configurations exist, which could simplify the measurement process and reduce the measurement uncertainties. Indeed, when the substrate consists of an insulating thick layer backed by a metal (an often encountered configuration), the so-called "thin film" regime can arise [8], [9], [10], [11], where the effect of back-reflections or partial decay of the e.m. field into the material under study can be completely neglected. In this situation, some useful simplifications of the model for the surface impedance are available. On the other hand, they are often exploited without paying due attention to their limitations and without evaluating the uncertainties that arise.

The aim of this work is to address these issues, extending upon the preliminary numerical evaluations provided in [11]. We thoroughly study when simplified models, which neglect the substrate contribution, can be used instead of the full model, identifying the situations in which the substrate properties yield negligible contribution to the ρ measurement and its uncertainty. To do so, we discuss the various sources of uncertainty, with the help of a brief description of typical measurement techniques. We show how the simplified models can greatly ease the extraction of the material resistivity from the measured surface impedance, with reduced uncertainty and also reduced computational cost for its evaluation.

The article is organized as follows. Section II provides the e.m. theoretical framework for the study of the surface impedance of different structures. Section III is devoted to the role of the substrate. In Section IV, the thin film regime is thoroughly studied, the various simplified model and the corresponding uncertainties are discussed, and the conditions for neglecting the substrate contribution are illustrated. A numerical study is then provided in Section V. In Section VI, some of the main experimental techniques used for the surface impedance measurements of planar structures are briefly recalled, providing the ground for discussing the sources of the uncertainty and for the presentation of the subsequent experimental case studies. Section VII reports experimental measurements of the surface impedance in different structures to exemplify the uncertainty evaluation and to provide a validation of the full and simplified models in the different regimes. Conclusions are drawn in Section VIII.

II. Surface Impedance

A. Definition

The *surface impedance*[1] is an important quantity when studying the incidence of an e.m. (e.m.) wave on the surface of a conductor. For an isotropic material, it is defined as (see [13], [14], [15])

$$\boldsymbol{E}_t = Z_s \boldsymbol{H}_t \times \hat{\boldsymbol{n}} \Rightarrow Z_s := \frac{|\boldsymbol{E}_t|}{|\boldsymbol{H}_t|} \tag{1}$$

where $\boldsymbol{E}_t$ and $\boldsymbol{H}_t$ are the electric and magnetic fields tangential to the surface and $\hat{\boldsymbol{n}}$ is the inward unit vector normal to the surface. The explicit expression of the surface impedance in terms of the material properties will be provided in Sections II-B, II-C, III, and IV. The used symbols are listed in Nomenclature.

We recall here some fundamental concepts related to the main approaches for surface impedance measurements at microwave frequencies. Considering the continuity of $\boldsymbol{H}_t$ and $\boldsymbol{E}_t$ at the surface, the surface impedance plays the important role of boundary condition for the determination of the fields immediately outside the conductor. For example, the electric field reflection coefficient Γ for a normally incident wave at the surface between vacuum and the conductor is computed as $\Gamma = (Z_s - Z_0)/(Z_s + Z_0)$ [15], [16], where $Z_0 := (\mu_0/\varepsilon_0)^{1/2} = 376.730\,313\,668(57)\,\Omega$ [17] is the intrinsic impedance of vacuum and where the number in parentheses is the numerical value of the standard uncertainty referred to the corresponding last digits of the quoted result.

The *surface resistance* $R_s = \mathrm{Re}(Z_s)$ is connected to the average power P_{diss} dissipated *per unit surface* in the conductor [15], which can be computed resorting to the Poynting vector theorem as the real part of the Poynting vector (time-averaged real power flowing into the conductor)

$$P_{\text{diss}} = \frac{1}{2}\,\mathrm{Re}(\boldsymbol{E_t} \times \boldsymbol{H_t^*} \cdot \hat{\boldsymbol{n}}) = \frac{1}{2} R_s |\mathbf{H_t}|^{\mathbf{2}}. \tag{2}$$

Similarly, the *surface reactance* $X_s = \mathrm{Im}(Z_s)$ is connected to the net reactive power in the conductor [16].

For simplicity's sake, isotropic media are considered so that all the material properties are scalars.

[1]Sometimes referred to as *intrinsic surface impedance* [12].

B. Bulk Expression

The explicit expression of the surface impedance exhibited by a semi-infinite conductor when a monochromatic TEM wave is normally[2] impinging on its flat[3] surface can be straightforwardly obtained imposing the continuity of the tangential components of the electric and magnetic field, whose ratio must, therefore, be equal to their ratio within the conductor. Since, in the semi-infinite conductor, the e.m. field propagates as a forward TEM wave, the ratio is by definition the *intrinsic impedance* of the medium

$$Z_{\text{intr}} := \sqrt{\frac{\mu}{\tilde{\varepsilon}}} \tag{3}$$

with $\tilde{\varepsilon} = \varepsilon - \mathrm{i}\sigma/\omega$ in the sinusoidal regime $e^{\mathrm{i}\omega t}$. The displacement currents are negligible with respect to conduction current in a good conductor at angular frequency ω in the microwaves and millimeter range (see [13], [16]) so that $\sigma/(\omega\varepsilon) \ll 1$. Hence, the surface impedance of an isotropic semi-infinite ("bulk") good conductor is equal to its intrinsic impedance with $\tilde{\varepsilon} \simeq -\mathrm{i}\sigma/\omega = -\mathrm{i}/(\omega\rho)$

$$Z_{\text{bulk}} := \sqrt{\mathrm{i}\omega\mu_0\rho} \tag{4}$$

where the magnetic permeability $\mu = \mu_0$ neglecting magnetic phenomena. The above expression holds in the local limit, where the *penetration depth* δ (when ρ is real, $\delta = (2\rho/(\omega\mu_0))^{1/2}$ [21]) of the exponentially attenuated e.m. fields is larger than the electron mean free path l. If the condition $l \ll \delta$ does not hold, the anomalous skin depth regime takes place [13]. The above treatment can be applied also to superconductors [19], where the local limit (see [22], [23], [24]) requires that $(l, \xi_0) \ll \min(\delta, \lambda)$ (see [25] and subsequent works for the combination of penetration depths). When conductors or superconductors of finite thickness t_s are considered, the above bulk expressions can be applied if $t_s \gg \delta$ or $t_s \gg \min(\delta, \lambda)$, respectively.

C. Multilayers

In thin films, i.e., $t_s \leq \delta$ or $t_s \leq \min(\delta, \lambda)$ for conductors or superconductors, the probing e.m. field reaches the substrate, possibly composed by many layers, experiencing multiple reflections/transmissions at each of the boundaries between different materials. The resulting e.m. problem can be studied resorting to the transmission line formalism [16], which yields the same results as those obtainable with a full study of the multiple reflections/transmissions [15]. An *effective surface impedance* Z_{eff} can be computed. In the following, for simplicity's sake, we assume TEM waves propagating along the direction normal to the layered structure.[4] In particular, the effective surface impedance $Z_{\text{eff}}^{(i)}$ (which is the input impedance in the transmission line formalism) at the interface with the ith layer (having thickness t_i, intrinsic impedance $Z_{\text{intr}}^{(i)}$, and propagation constant $k_i = \omega\mu_0/Z_{\text{intr}}^{(i)}$) is computed from the effective surface impedance $Z_{\text{eff}}^{(i-1)}$ exhibited at the input of the $(i-1)$th layer as follows:

$$Z_{\text{eff}}^{(i)} = Z_{\text{intr}}^{(i)} \frac{Z_{\text{eff}}^{(i-1)} + \mathrm{i}Z_{\text{intr}}^{(i)} \tan(k_i t_i)}{Z_{\text{intr}}^{(i)} + \mathrm{i}Z_{\text{eff}}^{(i-1)} \tan(k_i t_i)}. \tag{5}$$

By iteratively applying (5), which is called impedance transformation equation since it allows to "transform" the impedance value at one position along the transmission line to the impedance at another location, one can compute the effective surface impedance Z_{eff} of the whole multilayer.

A common measurement setup involves a thin conducting film grown on a substrate of finite thickness t_d and backed by a metal block of thickness much larger than the penetration depth [see sketch in Fig. 1(b)]. In this configuration, the expression of the effective surface impedance Z_{eff} can be particularized from (5) as

$$Z_{\text{eff}} = Z_{\text{intr}} \frac{Z_{s[\text{sub}]} + \mathrm{i}Z_{\text{intr}} \tan(k_s t_s)}{Z_{\text{intr}} + \mathrm{i}Z_{s[\text{sub}]} \tan(k_s t_s)} \tag{6}$$

where $k_s = \omega\mu_0/Z_{\text{intr}}$ is the wave propagation constant in the film having intrinsic impedance Z_{intr} and $Z_{s[\text{sub}]}$ is the (effective) surface impedance of the underlying substrate. Depending on the interplay of the various quantities (measuring frequency, thicknesses, resistivities, and dielectric permittivity), Z_{eff} can be significantly different from the bulk value Z_{bulk}, acquiring a dependence, potentially very pronounced, on the properties of the underlying layers.

For $|k_s t_s| \gg 1$ and $\operatorname{Im} k_s \neq 0$, i.e., bulk samples with finite losses, the above expression correctly reverts to the bulk one [see (4)]. Hence, (6) can be used with great generality.

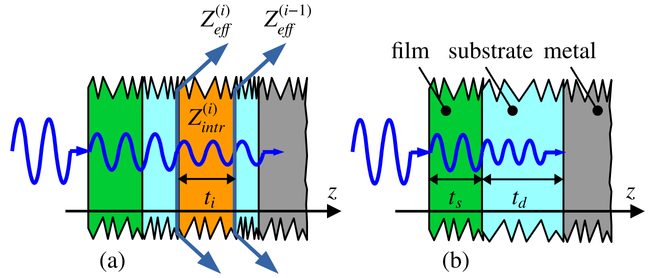

Fig. 1. (a) Sketch of a generic multilayer structure. (b) Sketch of a typical thin film structure: a (super)conducting film of thickness t_s is deposited onto a dielectric substrate of thickness t_d and backed by a thick (bulk) metal block.

[2]The extension to oblique incidence can be obtained by including the incidence angles [15] (see also [18] for a thorough study).

[3]That is, as long as e.m. field penetration depth is much smaller than the surface curvature radius [19]; otherwise, roughness effects' intervene [20].

[4]In many real setups (e.g., e.m. resonators or Corbino disk; see Section VI), waves are propagating in *guiding structures* [16] and, thus, are not free space TEM waves. Thus, the intrinsic impedance and propagation constant must be replaced by the specific wave impedance and wave longitudinal propagation constant. Moreover, in many cases, a change in geometry occurs at the surface between the guiding structure and the layered film (see Section VI) so that a full treatment requires cumbersome mode-matching approaches (see [26]). Nevertheless, it has been shown [27], [28] that the TEM approximation leads to similar results in typical measurement setups.

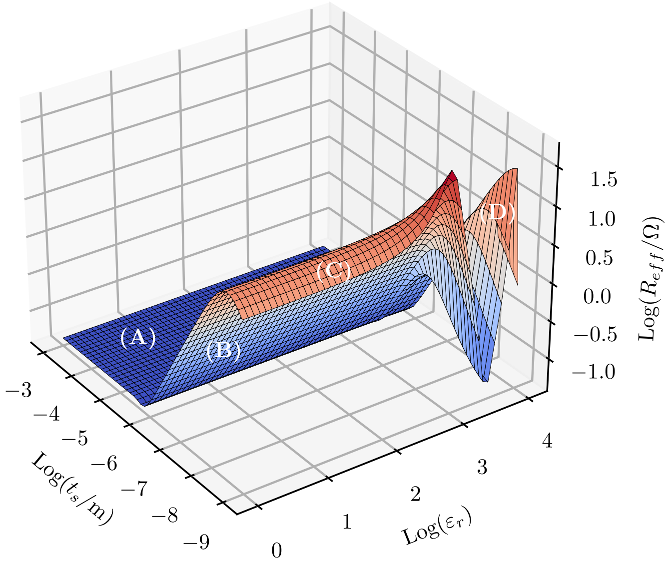

Fig. 2. Surface resistance $R_{\text{eff}} = \mathrm{Re}(Z_{\text{eff}})$ versus film thickness t_s and substrate relative permittivity ε_r for the layered structure described in the text.

D. Extraction of Resistivity From Z_{eff}

In many cases, a measurement of Z_s is a tool to obtain the material parameter ρ of a conductor. Since the substrate surface impedance $Z_{s[\text{sub}]}$ enters Z_{eff}, the extraction of ρ from Z_{eff} requires, in general, the separate knowledge of $Z_{s[\text{sub}]}$.

To illustrate the Z_{eff} dependence on the substrate properties, we refer as an example to a structure made by a tungsten W layer over an insulating substrate backed by bulk copper Cu. To reduce the parameter space extension, we take t_s and ε_r within the ranges $(10^{-9}$–$10^{-3})$ m and 1–10^4, respectively, and keep fixed all the other quantities. In particular, we take the metals' d.c. conductivity $\rho_{Cu} = 1.68 \times 10^{-8}\,\Omega\,\mathrm{m}$ [29] and $\rho_W = 5.6 \times 10^{-8}\,\Omega\,\mathrm{m}$ [30] (room temperature values), zero losses ($\tan\delta_\varepsilon = 0$) and $t_d = 0.25\,\mathrm{mm}$ thickness for the insulating substrate, and frequency $\nu = 10\,\mathrm{GHz}$. Despite this specific choice, which is made to adhere to realistic situations and also to make apparent all the desired features in the chosen value ranges, the obtained results are qualitatively general. We focus on the surface resistance $R_{\text{eff}} = \mathrm{Re}(Z_{\text{eff}})$, plotted in Fig. 2. It can be seen that the R_{eff} surface can be roughly divided into four regions, marked (A)–(D) in the plot, where different trends and features appear. In region (A), R_{eff} is independent of t_s and ε_r. In particular, the t_s-independence means that the film is actually in the bulk limit, i.e., $t_s \gg \delta = 1.2\,\mu\mathrm{m}$, and thus, (6) reverts to (4). In region (B), the film is thinner, and R_{eff} is $\propto t_s^{-1}$ and independent of ε_r: although far from the bulk limit, this regime is characterized by substantial independence of R_{eff} from the substrate properties (hence, not limited to ε_r selected to draw the plot), which is a useful property widely encountered in the experiments. In region (C), R_{eff} is no more $\propto t_s^{-1}$ becoming instead strongly dependent on the substrate properties, in particular, on its thickness (here not shown since the plot has been produced at fixed t_d). Finally, in region (D) (small film thickness and high substrate ε_r), R_{eff} shows pronounced oscillations by varying any of the properties of the layered structure [analytically, this behavior is due to the presence of the "$\tan$" terms in (6)]. This example allows identifying region (B) as the region where the measured surface impedance, albeit different from the bulk value, does not depend on the substrate properties. In the following sections, a thorough study of the effective surface impedance of typical substrates (see Section III) is done to provide the bases for the subsequent analyses of the thin film regime, made through an analytical study of the expression of Z_{eff} (see (6) and Section IV) and by a numerical study of realistic scenarios (Section V).

III. Substrate Surface Impedance

Since the analytical conditions for the thin film regime for Z_{eff} rely on the substrate surface impedance $Z_{s[\text{sub}]}$ being "large," we first discuss the latter, which can vary in a quite large range depending on the substrate materials and structure.

Metal Substrate: An extreme limit is given by the absence of the dielectric altogether. The substrate is then a bulk metal of resistivity ρ_m, for which (4) applies

$$Z_{s[\text{sub}]} = Z_{\text{bulk}} = \sqrt{\mathrm{i}\omega\mu_0\rho_m} =: Z_m. \tag{7}$$

For Cu at room temperature, $Z_m = 25.8(1+\mathrm{i})\,\mathrm{m}\Omega$ at $\nu = 10\,\mathrm{GHz}$. An exemplifying application is represented by the coated superconductor tapes, in which thin (super)conducting films are grown on metallic substrates [31].

A. Purely Dielectric Substrate

Another limit is given by an ideally infinitely thick dielectric. In the vacuum (isolated film), $Z_{s[\text{sub}]} = Z_0$, the free space impedance. For lossless semi-infinite insulator (real ε_r), one has from (3)

$$Z_{s[\text{sub}]} = Z_{\text{intr}} = Z_0/\sqrt{\varepsilon_r} =: Z_d. \tag{8}$$

B. Dielectric Substrate Over Metal Plate

More often, the substrate consists of a layered structure in which an insulating, dielectric, material of thickness t_d is backed by a thick (i.e., equivalent to a semi-infinite) conductor having impedance Z_m. A typical case is a conducting film grown on some substrate and inserted in a radiation screening case. In this general case, the *effective* $Z_{s[\text{sub}]}$ can be computed through the usual impedance transformation [see (6)] rewritten for the present situation

$$Z_{s[\text{sub}]} = Z_{\text{eff}} = Z_d \frac{Z_m + \mathrm{i}Z_d\tan(k_d t_d)}{Z_d + \mathrm{i}Z_m\tan(k_d t_d)} \tag{9}$$

where $k_d = \omega\mu_0/Z_d$ is the wave propagation constant in the dielectric. Some common dielectric materials are PTFE, quartz, sapphire, $SrLaAlO_4$, and $SrTiO_3$, with (transverse) permittivity $\varepsilon_r = 2.22$, 4.44, 9.4, 16.8, and 30, respectively [32], [33], [34]. Commercially available dielectric substrate thicknesses are typically 0.1, 0.5, and 1 mm [35].

In almost all practical cases, $|Z_m| \ll |Z_d|$. When additionally $k_d t_d \neq n\pi/2$, expression (9) simplifies to

$$Z_{s[\text{sub}]} \simeq \mathrm{i}Z_d\tan(k_d t_d) \tag{10}$$

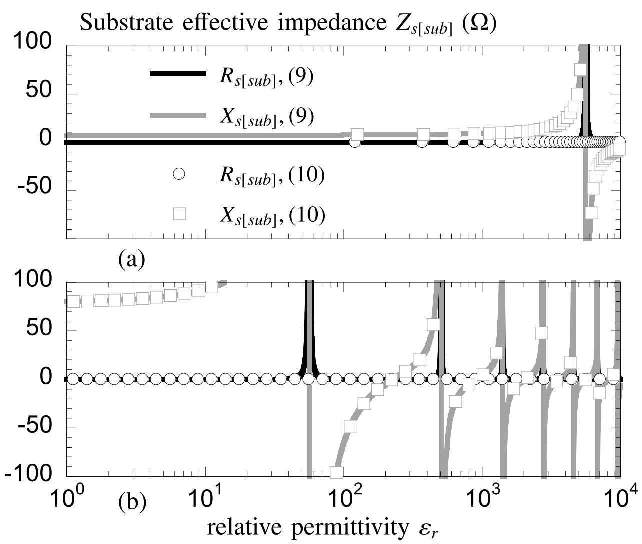

Fig. 3. Substrate effective impedance $Z_{s[\text{sub}]}$ versus relative permittivity ε_r. Numerical values: substrate thickness $t_d = 0.5$ mm; backing metal: Cu at room temperature; and frequency: (a) 2 GHz and (b) 20 GHz.

which, for lossless dielectrics, is a purely imaginary quantity depending only on two material parameters ε_r and t_d and on the measuring parameter ω. This is a particularly useful expression to qualitatively understand the behavior of $Z_{s[\text{sub}]}$. For example, through this expression it is easy to recognize the so-called substrate antiresonance/resonance conditions $k_d t_d = n\pi/2$, where the term $\tan(k_d t_d)$ diverges or vanishes, respectively. For the resonance condition, $k_d t_d = n\pi$, the approximated (10) yields zero, whereas (9) yields Z_m. In the antiresonance condition, $k_d t_d = \pi/2 + n\pi$, the approximated (10) diverges instead of yielding the (large modulus) value $Z_{s[\text{sub}]} \to Z_d^2/Z_m$ given by (9). In real situations, given a fixed substrate thickness t_d, the resonance condition can be attained either by varying the measurement frequency [36] or by changing the sample temperature if the dielectric has a pronounced temperature variation of ε_r, like $SrTiO_3$ [37]. As we will show in V and VII-D, this property can have important consequences on experiments.

A numerical example of the appearance of substrate resonances in $Z_{s[\text{sub}]}$ is shown in Fig. 3, in which $Z_{s[\text{sub}]}$ is computed through (9) for two selected frequencies (2 GHz and 20 GHz, figures (a) and (b), respectively) with a *real* (lossless case) relative permittivity $1 \leq \varepsilon_r \leq 10^4$. The substrate thickness is fixed at $t_d = 0.5$ mm, and the backing metal is taken as Cu at room temperature. In addition, the approximated (10) is also plotted. As anticipated, it can easily be seen that this expression reproduces the full expression (9), apart from the antiresonances ($\tan(k_d t_d) \to \infty$) and resonances ($\tan(k_d t_d) \to 0$), where it differs yielding divergent values and zero values (not visible in the plot scale), respectively.

We mention that a much more intricate scenario arises when semiconducting substrates are involved [38]. In this situation, both real and imaginary parts of $Z_{s[\text{sub}]}$ change significantly with doping, temperature, and frequency, which impacts on the conductivity potentially making it dominant with respect to ε_r. This scenario is briefly exemplified in Section VII-C.

IV. (Super)conductor Surface Impedance: Thin Film Regime

Equation (6) represents a transcendental, fractional, and irrational complex function of the complex variable ρ ($\rho \in \mathbb{C}$ in superconductors). As such, it does not allow an analytical inversion, and its high nonlinearity makes a first-order Taylor expansion potentially insufficient for the computation of the uncertainty $u(\rho)$. Thus, in many cases, a Monte Carlo approach would be required, making the uncertainty evaluation very time-consuming considering that: 1) each measurement set typically consists of many data points and 2) Z_s and ρ are complex quantities [39], [40]. Moreover, the uncertainty on a typical measurement can have a large contribution that stems from the accuracy with which the geometry is known (thicknesses t_s and t_d), as well as from the accuracy in the determination of ε_r, with the substrate parameters often badly determined. Hence, it is important to determine the regimes where the substrate contribution can be neglected, enabling a reduced impact [i.e., low sensitivity coefficients for $u(\rho)$] of the potentially high uncertainties on the substrate properties. Regimes with negligible substrate contribution and the corresponding simplified models were developed through time [8], [9], [10], [41]. However, the uncertainties on ρ arising from the use of simplified models were often overlooked, and no systematic discussion about the various applicable regimes is provided. In order to fill this gap, in this section, we present the thin film regime with the main simplified models, the analytical and physical conditions of applicability, and the expressions of the measurement uncertainties.

A. Bulk Regime

We repeat here for completeness, and without further comments, the expression of the surface impedance that is obtained for an infinitely extended material, i.e., having $t_s \gg |\delta|$ ($t_s \gg \max(|\delta|, \lambda)$ for superconductors) is

$$Z_s = Z_{\text{bulk}} = \sqrt{\mathrm{i}\omega\mu_0\rho}. \tag{11}$$

The uncertainty on ρ can be easily evaluated

$$u(\mathrm{Re}(\rho)) = \frac{R_s X_s}{\mu_0 \pi \nu}\sqrt{\frac{u^2(\nu)}{\nu^2} + \frac{u^2(R_s)}{R_s^2} + \frac{u^2(X_s)}{X_s^2}} \tag{12a}$$

$$u(\mathrm{Im}(\rho)) = \frac{R_s X_s}{\mu_0 \pi \nu}\sqrt{\frac{(R_s^2 - X_s^2)^2}{4R_s^2 X_s^2}\frac{u^2(\nu)}{\nu^2} + \frac{u^2(R_s)}{X_s^2} + \frac{u^2(X_s)}{R_s^2}} \tag{12b}$$

where $u(\mu_0)$ is neglected [17] and the correlations between $u(R_s)$ and $u(X_s)$ are also neglected (here and in all the similar following equations) for the sake of compactness. It is worth noting that when only the real part of Z_{bulk} is measured because of experimental limitations (see Section VI), one obtains only the real part of the square root of the complex ρ without being able to separately ascertain the real or imaginary parts of ρ. This contrasts with what happens in the thin film regime, where $\mathrm{Re}(Z_s)$ can directly yield $\mathrm{Re}(\rho)$; see Section IV-C.

B. Intrinsic Film Regime

Despite the (over)use of the term "intrinsic," this regime deals mainly with films of finite thickness and is based on the comparison of different impedances. When

$$\frac{|\tan(k_s t_s)||Z_{\text{intr}}|}{|Z_{s[\text{sub}]}|} \ll 1 \text{ and} \tag{13a}$$

$$\frac{|\cot(k_s t_s)||Z_{\text{intr}}|}{|Z_{s[\text{sub}]}|} \ll 1 \tag{13b}$$

(6) simplifies yielding the *intrinsic film impedance* [8], [9], [10]

$$Z_s = Z_{\text{eff}} \simeq -\mathrm{i}Z_{\text{intr}} \cot(k_s t_s) =: Z_{\text{si}}. \tag{14}$$

The conditions (13) are met if the film is thin enough, far away from the antiresonance/resonance conditions. Physically, it implies that the substrate is so mismatched with respect to the film impedance that a total reflection of the e.m. field occurs at the film-substrate interface. Z_{si} depends exclusively on the film properties, and it has the advantage of having a large range of applicability (see Section V-A). Indeed, it is worth noting that also high conductive films (small $|Z_{\text{intr}}|$), even if thick (high t_s), can meet the conditions (13), yielding, in this case, $Z_{\text{intr}} \to Z_{\text{bulk}}$. This means that expression (14) can capture both the bulk regime, the thin film regime, and the crossover between them. With respect to the simpler thin film expression, discussed later, (14) has the disadvantage of not being analytically invertible. When used to extract the material resistivity ρ from an experimentally measured Z_s, (14) must, thus, be numerically inverted. Symbolically,

$$\rho = Z_{\text{si}}^{-1}(Z_s; t_s) \tag{15}$$

where the superscript "-1" denotes the inverse function and the main needed quantities are made explicit. By using (15) instead of the full model (6), an approximation error $\Delta\rho_a$ appears

$$\Delta\rho_a = Z_{\text{eff}}^{-1}(Z_s; t_s, Z_{s[\text{sub}]}) - Z_{\text{si}}^{-1}(Z_s; t_s). \tag{16}$$

Its uncertainty contribution $u(\Delta\rho_a)$ enters $u(\rho)$:

$$u(\mathrm{Re}(\rho)) = \left[\left(\frac{\partial \,\mathrm{Re}(Z_{\text{si}}^{-1})}{\partial R_s} u(R_s)\right)^2 + \left(\frac{\partial \,\mathrm{Re}(Z_{\text{si}}^{-1})}{\partial X_s} u(X_s)\right)^2 + \left(\frac{\partial \,\mathrm{Re}(Z_{\text{si}}^{-1})}{\partial t_s} u(t_s)\right)^2 + u^2(\mathrm{Re}(\Delta\rho_a))\right]^{1/2} \tag{17a}$$

$$u(\mathrm{Im}(\rho)) = \left[\left(\frac{\partial \,\mathrm{Im}(Z_{\text{si}}^{-1})}{\partial R_s} u(R_s)\right)^2 + \left(\frac{\partial \,\mathrm{Im}(Z_{\text{si}}^{-1})}{\partial X_s} u(X_s)\right)^2 + \left(\frac{\partial \,\mathrm{Im}(Z_{\text{si}}^{-1})}{\partial t_s} u(t_s)\right)^2 + u^2(\mathrm{Im}(\Delta\rho_a))\right]^{1/2}. \tag{17b}$$

It is apparent that the use of the simplified model (15) is acceptable, consistently with the prescription of [42], if $\Delta\rho_a$ and $u(\Delta\rho_a)$ are much smaller than $u(\rho)$, considering separately the real and imaginary parts. While (13) provides the analytical conditions to be met, actual quantification is provided in the numerical study discussed in Section V-A and in the experimental data analysis exemplified in Section VII-B.

C. Thin Film Regime

We consider the simple case

$$\frac{t_s}{|\delta|} \ll 1, \text{for conductors}$$
$$\frac{t_s}{\min(|\delta|, \lambda)} \ll 1, \text{for superconductors.} \tag{18}$$

Then, $\tan(k_s t_s) \to k_s t_s$, and (6) becomes

$$Z_s = Z_{\text{eff}} \simeq Z_{\text{sf}} \frac{Z_{s[\text{sub}]} + \mathrm{i}\omega\mu_0 t_s}{Z_{\text{sf}} + Z_{s[\text{sub}]}}, \text{with } Z_{\text{sf}} := \frac{\rho}{t_s} \tag{19}$$

where Z_{sf} is the so-called *thin film impedance*. Neglecting momentarily the term $\mathrm{i}\omega\mu_0 t_s$ (which is indeed often negligible for small t_s), (19) simply represents the parallel of the impedances Z_{sf} and $Z_{s[\text{sub}]}$. As such, it is easily invertible, allowing to compute Z_{sf} and ρ from the measured Z_s and t_s and the knowledge of $Z_{s[\text{sub}]}$. If

$$\frac{\omega\mu_0 t_s}{|Z_{s[\text{sub}]}|} \ll 1, \text{and} \tag{20a}$$

$$\frac{|Z_{\text{sf}}|}{|Z_{s[\text{sub}]}|} \ll 1 \tag{20b}$$

where condition (20a) is often verified for dielectric substrates outside the resonance condition (but not verified for bulk metallic substrates), (19) simplifies further to Z_{sf} itself

$$Z_s \simeq Z_{\text{sf}} = \frac{\rho}{t_s}. \tag{21}$$

It can be noted that conditions (20a) and (20b) correspond to conditions (13a) and (13b), respectively, rewritten in the simplified form taking advantage of condition (18). Physically, with respect to the intrinsic film regime, in the thin film regime, any phase change due to the e.m. propagation in the film is negligible. This is a very useful limit since, in this case, the measured Z_s depends only, and in a simple way, on the thin film properties so that ρ can be easily computed

$$\rho = Z_s t_s. \tag{22}$$

Nevertheless, for very thin films, caution should be paid on condition (20b) since very small t_s yields divergent Z_{sf} ultimately making the condition not satisfied.

Analogously to the intrinsic film regime, the approximation error and the overall uncertainty can be written down as

$$\Delta\rho_a = Z_{\text{eff}}^{-1}(Z_s; t_s, Z_{s[\text{sub}]}) - Z_s t_s \tag{23}$$

and

$$u(\mathrm{Re}(\rho)) = \sqrt{t_s^2 u(R_s)^2 + R_s^2 u(t_s)^2 + u^2(\mathrm{Re}(\Delta\rho_a))} \tag{24a}$$

$$u(\mathrm{Im}(\rho)) = \sqrt{t_s^2 u(X_s)^2 + X_s^2 u(t_s)^2 + u^2(\mathrm{Im}(\Delta\rho_a))}. \tag{24b}$$

In comparison with the intrinsic film impedance, the thin film impedance model has a stricter range of applicability, requiring smaller t_s than the former (see the following section). On the other hand, its simpler form with respect to the intrinsic film impedance (14) allows for straightforward calculations and allows also to compute separately $\mathrm{Re}(\rho)$ and $\mathrm{Im}(\rho)$ (and their uncertainties) from the measured R_s and X_s. When the experiment yields more accurate R_s measurements than the X_s ones (see Section VI), the possibility to extract an accurate $\mathrm{Re}(\rho)$ from R_s only is a clear advantage.

V. Numerical Computations for Z_{eff}

A. Comparison Between Full and Simplified Models

In this section, we provide an evaluation of the approximation error $\Delta\rho_a$ in the determination of ρ, which would be needed to include substrate effects in the simplified models of (14) and (21). In order to make contact with the experiments, we numerically compute Z_{eff} starting from ρ in different regions of the parameter space, and then, we take $Z_s = Z_{\mathrm{eff}}$ and invert it by means of the two expressions for Z_{si} and Z_{sf} [see (14) and (21)]. We, thus, evaluate the normalized approximation error

$$\Delta\rho_{a\%} = \left(\frac{\mathrm{Re}(\Delta\rho_a)}{\mathrm{Re}(\rho)}\right) + \mathrm{i}\left(\frac{\mathrm{Im}(\Delta\rho_a)}{\mathrm{Im}(\rho)}\right) \tag{25}$$

where $\Delta\rho_a$ is defined in (16) and (23) for the two different regimes. For a given ρ, we also compare how much Z_{si} or Z_{sf} differs from Z_{eff} by computing the relative deviations

$$\Delta Z_{a\%} = \frac{\mathrm{Re}(Z - Z_{\mathrm{eff}})}{\mathrm{Re}(Z_{\mathrm{eff}})} + \mathrm{i}\frac{\mathrm{Im}(Z - Z_{\mathrm{eff}})}{\mathrm{Im}(Z_{\mathrm{eff}})} \tag{26}$$

where Z stands for Z_{si} or Z_{sf}. Since the functions in (26) are the inverse of those appearing in (25), it is easy to show that for small deviations $|\Delta\rho_{a\%}| \ll 1$, and for the same parameters, $\Delta\rho_{a\%} \simeq \Delta Z_{a\%}$. This fact, exemplified in the following plots, is useful in the evaluation of $\Delta\rho_{a\%}$ from a measured ρ since $\Delta Z_{a\%}$ is more easily computed.

Preliminary considerations must be made concerning the relevant parameters. The parameter space is extremely extended: there are three parameters for the substrate ($\mathrm{Re}(\varepsilon_r)$, $\tan\delta_\varepsilon$, and t_d), three parameters for the thin film (the complex ρ and t_s), and the measuring parameter (the frequency) ν for a total of seven independent parameters. In order to reduce the parameter space, we keep t_s and ν as independent variables: t_s is taken between $1\,\mathrm{nm}$ and $100\,\mu\mathrm{m}$, to justify the concept of "thin film," and ν in the (0.5–50)-GHz range, to cover the microwave to millimeter-wave range. We then select typical values for the dielectric substrate backed by a bulk metal, covering a wide range of $Z_{s[\mathrm{sub}]}$. Following the discussion made in Section III, we take $t_d = 0.75\,\mathrm{mm}$ and $LaAlO_3$ as dielectric substrate, with $\varepsilon_r = 23.70$ and 23.97 at room and cryogenic temperatures, respectively, and negligible losses [34]. Other dielectric materials (sapphire and rutile), with smaller and higher ε_r than $LaAlO_3$, were considered in [11], showing that the same qualitative features appear. Concerning the thin film materials, in order to illustrate two very different situations, we consider both a normal conductor (Cu at room temperature) and a superconductor (in zero magnetic fields), having real and mainly imaginary resistivities, respectively. The superconductor resistivity is described by the

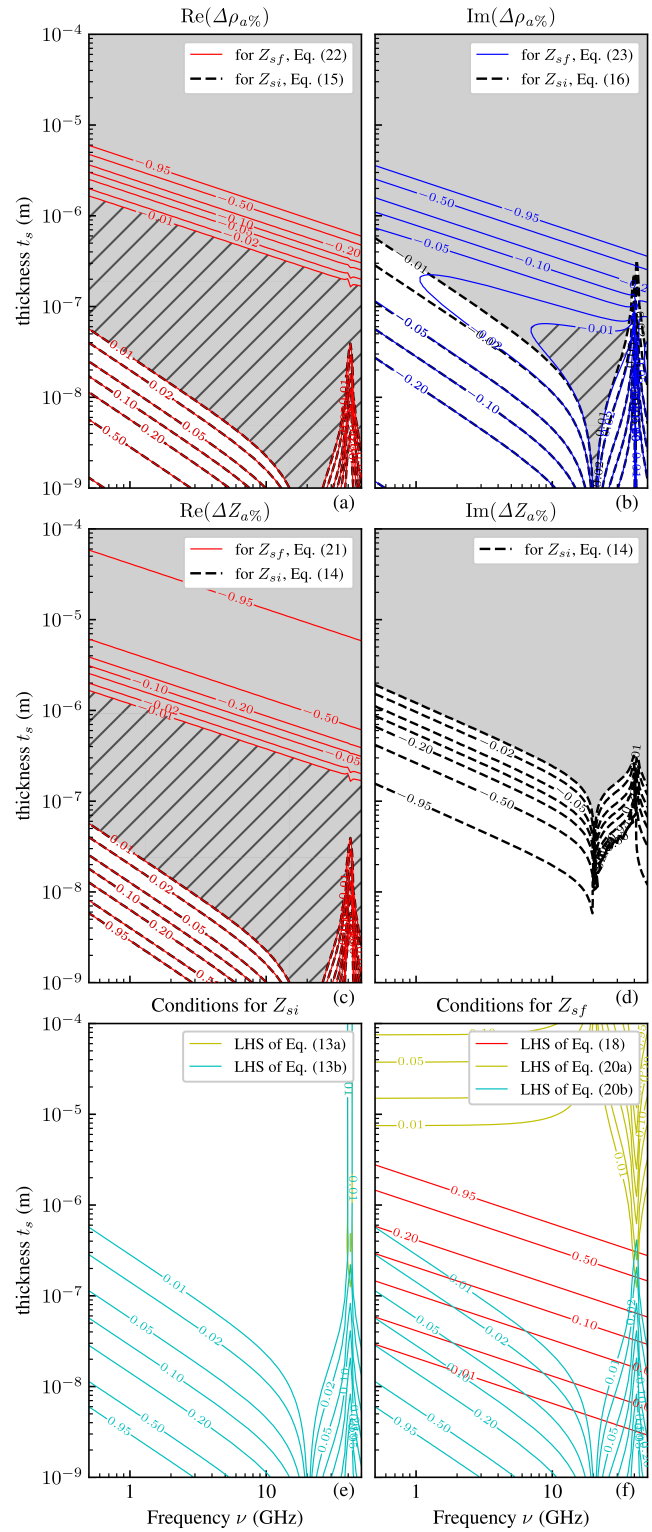

Fig. 4. Contour plots for the thin film regime study of Cu at room T. (a) and (b) Real and imaginary parts of (25). (c) and (d) Real and imaginary parts of (26). In (a)–(d), the gray/hatched areas denote regions where the approximation error is in modulus < 0.01 for Z_{si} and Z_{sf}, respectively. (e) and (f) Conditions for the application of the Z_{si} and Z_f models; "LHS" stands for left-handed size.

well-known two-fluid model [43]

$$\frac{1}{\rho} = \frac{1}{\rho_n}(T/T_c)^\alpha - \mathrm{i}\frac{1-(T/T_c)^\alpha}{\mu_0\omega\lambda_0^2} \tag{27}$$

where T_c is the critical temperature below which the material superconducts, ρ_n is the normal state (real) resistivity, λ_0 is the zero-temperature London penetration length, and $\alpha = 2$ gives a reasonable semiquantitative description of real data (we avoid here more complicated, material–specific expressions). In order to describe a practical, mainly reactive film, in the following, we will use this model with material parameters typical of high-T_c superconductor $YBa_2Cu_3O_{7-\delta}$ (YBCO): $T_c = 92\,\mathrm{K}$, $\rho_n = 1.0 \times 10^{-6}\,\Omega\,\mathrm{m}$ [44], and $\lambda_0 = 150\,\mathrm{nm}$ [43], at $T = 77\,\mathrm{K}$ (liquid nitrogen temperature).

Figs. 4 and 5 are the main results of this section. There, in (a) and (b), we plot the normalized $\mathrm{Re}\,(\Delta\rho_a)$ and $\mathrm{Im}\,(\Delta\rho_a)$, respectively, in terms of isolevel lines for both Z_{si} (black dashed thick lines) and Z_{sf} (colored continuous thin lines), respectively. Values above $|0.95|$ are not reported. Hatched and gray areas correspond to an approximation error of less than 0.01 in modulus with respect to Z_{si} or Z_{sf}, respectively.

Several general aspects can be commented. First, the hatched/gray regions of the figures identify the parameter space for the applicability of the simplified models. There the approximation errors are indeed smaller than the typical 1%–10% experimental uncertainties (see Section VI). We need to assess also that the uncertainty on the approximation error is negligible with respect to the experimental uncertainties. This can be easily done considering regions (A) and (B) of Fig. 2, which exemplify that the sensitivity of R_s (and analogously of X_s) on the substrate properties is vanishingly small.

Second, in the lower left part of Figs. 4 and 5 [(a)–(d)], it can be seen that the iso-curves referring to Z_{si} and Z_{sf} superimpose: in this region of the $\{\nu,\ t_s\}$ plane, the two models are completely equivalent. Moreover, Z_{si} and Z_{sf} consistently provide an underestimate of the correct values. By contrast, in the upper part of the same figures, the approximation error by using Z_{si} remains consistently below 1%, whereas, for Z_{sf}, it steeply increases.

Third, by comparing the normalized approximation error on ρ (25), plotted in Fig. 4(a) and (b), to the normalized deviations on Z_s (26), plotted in Fig. 4(c) and (d), it can be seen that for small values, their isolevel curves superimpose.

Fourth, it can be noted that the parameters ν and t_s have a nontrivial influence, due to the possible resonances of the substrate, as apparent in the lower right part (high frequency and small thickness) of Figs. 4 and 5(a)–(d), where the approximation error due to the simplified models is large.

We now provide a quantification of the conditions for the applicability of the simplified models: again considering Figs 4 and 5, the left-hand side (LHS) ratios of (13) are plotted in (e) and those of (18) and (20) in (f). Indeed, it can be seen that depending on the situations, values 0.2-0.10 for the ratios, (e) and (f), correspond to negligible approximation errors, below 1%, (a)–(d). Moreover, (f) shows that the thin film condition alone (18), which is the most easily evaluated, allows to locate the hatched (small approximation error) regions, once the substrate resonances are avoided.

A remark can be made concerning the slopes of the iso-level curves for a normal metal with respect to a superconductor: they differ since $\delta \propto \nu^{-1/2}$ for the former and constant λ for the latter.

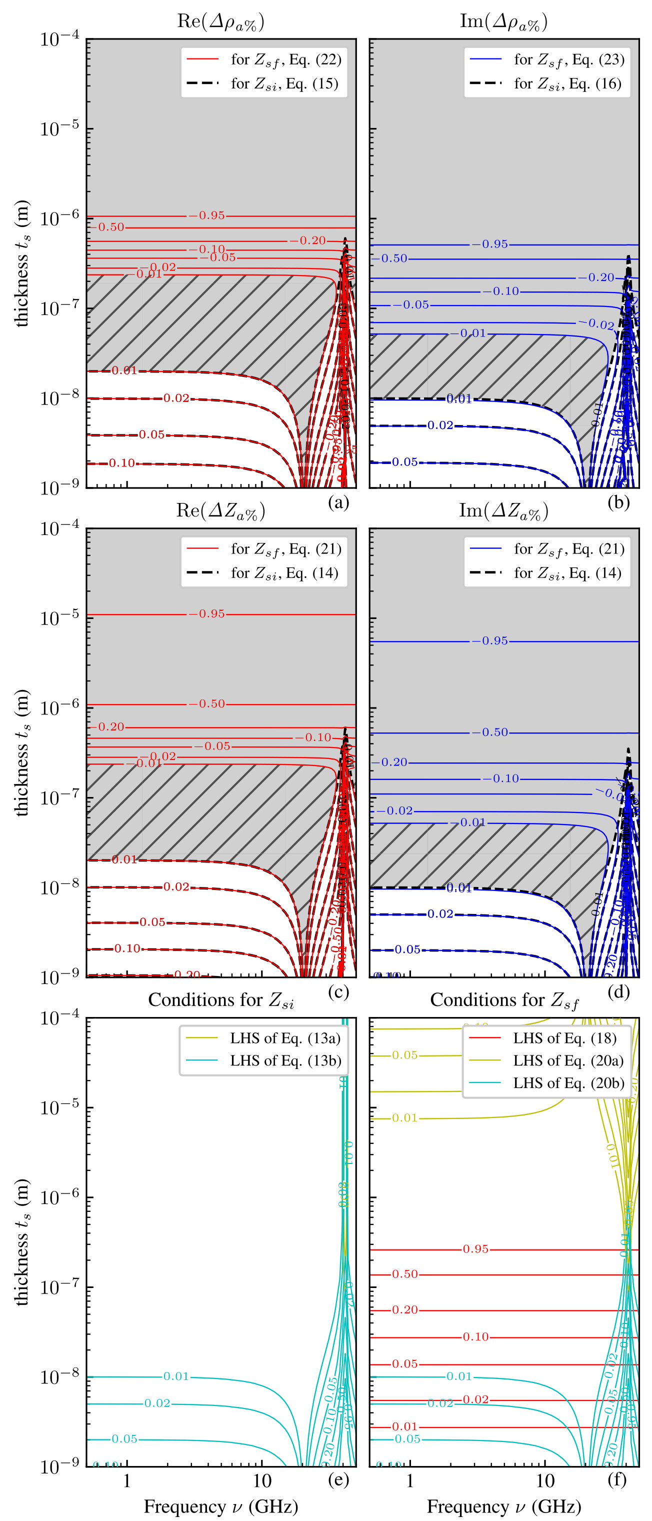

Fig. 5. Contour plots with labeled isolevel curves for the thin film regime study of a superconducting $YBa_2Cu_3O_{7-\delta}$. Figures as in Fig. 4.

Summarizing, the approximation error that arises from the use of the simplified expressions instead of the full (6) can be very large for very thin films, or at low frequency, a result that is not necessarily intuitive. On the other hand, there is a wide region of the parameter space where the use of the extremely simple thin film model of (22) implies an approxi-

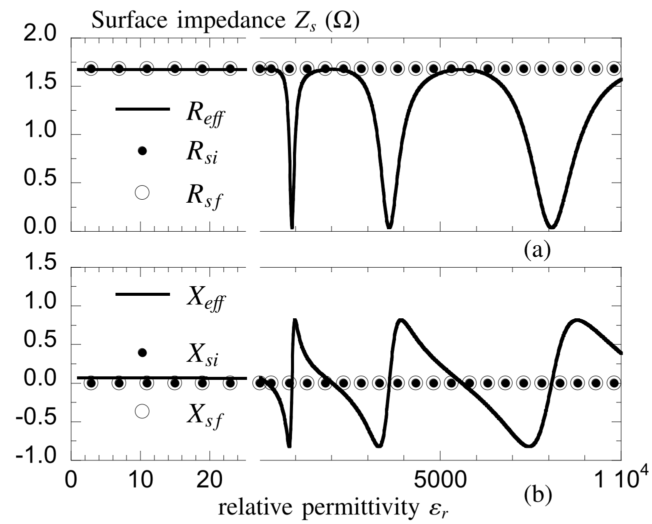

Fig. 6. Comparison of Z_{eff}, Z_{si}, and Z_{sf} in function of the substrate ε_r in a normal conducting (Cu, resistive) thin film. (a) Surface resistance; at low ε_r, the simplified expressions reproduce well R_{eff}, and as a general rule, they overestimate it. (b) Surface reactance.

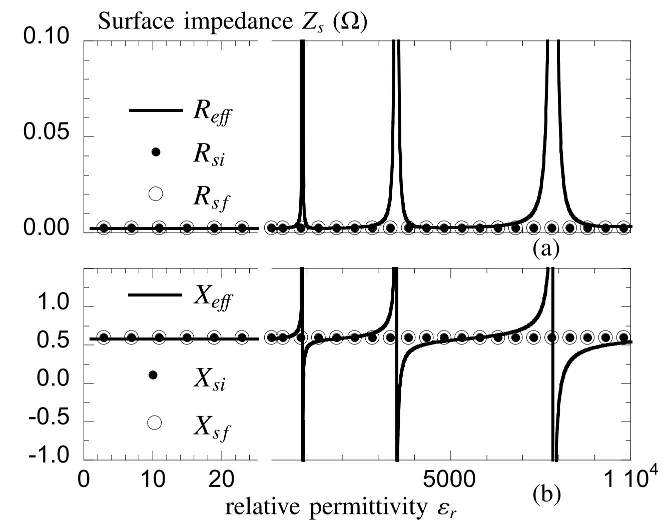

Fig. 7. Comparison of Z_{eff}, Z_{si}, and Z_{sf} in function of the substrate ε_r in a superconducting (YBCO, mainly reactive) thin film. (a) Surface resistance; at low ε_r, the simplified expressions reproduce well R_{eff}, and as a general rule, they underestimate it. (b) Surface reactance.

mation error below 1%, negligible compared to experimental uncertainties, typically $\sim 1\%$–10% in cryogenic environments (see Section VI). Finally, we have shown that the a priori identification of the $\{\nu,\ t_s\}$ region where simplified models can be used is not trivial and can often require a careful evaluation of the substrate impedance. In particular, the substrate resonances heavily influence the surface impedance and can potentially jeopardize the interpretation of the experimental data. In Section V-B, we focus on the effect of such substrate resonances.

B. Effect of Substrate Resonances in Thin Films

We now focus on the situation in which the substrate undergoes resonance phenomena, as those described in Section III and mentioned in Section V-A. This will allow us to highlight: 1) how much substrate resonances are detrimental to the extraction of ρ within the thin film model and 2) a specific feature that will allow us to experimentally validate (6) in such extreme conditions. To this end, we consider a thin conductive film over a finite thickness ($t_d = 0.5\,\text{mm}$) layer of $SrTiO_3$, a ferroelectric material commonly used for substrates, backed by a metal (structure as in Fig. 1). The dielectric ε_r changes severely (by orders of magnitude) with the temperature T, thus causing with certainty the substrate resonances. For the thin film, we consider again both the normal conductor and the superconductor already described in the previous Section V-A, at fixed thickness $t_s = 10\,\text{nm}$ and fixed frequency $\nu = 10\,\text{GHz}$. Fig. 6 reports numerical results for Z_{eff} [see (6)] compared with the expressions Z_{si} and Z_{sf} for the Cu film on a dielectric with varying ε_r. Looking at the real parts [see (a)], it can be seen that the simplified expressions yield the same results as the full Z_{eff} at low ε_r, whereas, by increasing ε_r, significant discrepancies arise because of the substrate resonances. We stress that in this case, the simplified expressions systematically *overestimate* the surface resistance with respect to the full expression. The behavior of the imaginary part [see (b)] is reported for completeness, but we remark that the comparison is not particularly meaningful: since ρ is real, $X_{\text{sf}} = 0$ and $X_{\text{si}} \sim 0$, and therefore, (14) and (21) cannot reproduce values different from 0. We now move to the case of the superconducting (mainly reactive) film. Numerical results are reported in Fig. 7 with the same ε_r variation as for the Cu film. Similar considerations apply: the simplified models yield the same results as Z_{eff} at low ε_r, and the largest discrepancies appear at the substrate resonances. However, a striking difference emerges, entirely due to the important reactive contribution to the conductivity: the surface resistance as calculated by the simplified expressions now systematically *underestimates* the results as obtained from the full calculation. This feature allows for a direct experimental validation (see Section VII-D) of the results up to now obtained: by increasing $\text{Re}(\sigma)$ of a superconducting film in the vicinity of a substrate resonance, one should observe a change from dips to peaks in its R_s.

VI. Experimental Techniques

A thorough presentation of the experimental techniques is given in [45]. We focus here on a very wideband (decades in frequency) technique, the so-called Corbino disk [28], [46], [47], and on the single-frequency, high-sensitivity dielectric resonator technique [48], [49], [50], [51], which can be extended to a few multiple frequencies in some cases [3], [52], [53], [54], [55]. The purpose is to highlight the main uncertainty sources in Z_s measurements due to the technique's peculiarities.

A. Corbino Disk

In the Corbino disk setup, the flat sample to be measured is placed as the termination load of a coaxial cable [see Fig. 8(a)]. The measurement of the complex reflection coefficient Γ of

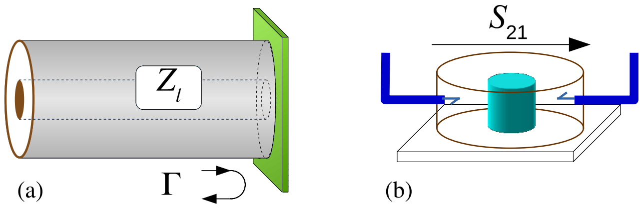

Fig. 8. Sketch of the experimental setups. (a) Corbino disk setup with a coaxial cable terminated on the sample (in green). (b) Cylindrical dielectric-loaded resonator with one base occupied by the sample (in green).

the impinging TEM wave at the sample location

$$\Gamma = \frac{Z_s - Z_l}{Z_s + Z_l} \tag{28}$$

straightforwardly yields the sample surface impedance Z_s once the wave impedance of the coaxial line Z_l, typically real, is known.[5] Since guided TEM fields are involved, $Z_l = Z_{\text{intr}} = Z_0/(\varepsilon_r)^{1/2}$ of the insulating medium of the coaxial cable (typically PTFE, $\varepsilon_r = 2.22$ [32]), and the line can be operated between d.c. (often limited to 1–2 GHz due to contact parasitic capacitances) up to the cutoff frequency of the higher order e.m. modes of the line (a few tens of GHz). In actual measurements, an important issue concerns the calibration of the measurement line connecting the instrument [a vector network analyzer (VNA)] to the sample. Indeed, the connection line, with scattering (complex) coefficient S_{ij}^{line}, relates Γ to Γ_m measured by the VNA [16], [28]

$$\Gamma_m = S_{11}^{\text{line}} + \frac{S_{21}^{\text{line}} S_{12}^{\text{line}} \Gamma}{1 - S_{22}^{\text{line}} \Gamma}. \tag{29}$$

The calibration yielding S_{ij}^{line} requires measurements to be performed with known standards in the same conditions (including the temperature) of the measurements of interest. This is not always possible at cryogenic temperatures, required, e.g., for measurements on superconductors; hence, various approximated calibration schemes have been devised [28], [46], [47], [56], [57], which typically limit the highest frequency accessible to around 20–30 GHz. In these schemes, often the a priori known or negligible impedances of the sample under measurement in particular states (e.g., minimum achievable temperatures or superconductors in the normal state with respect to the superconducting state) are exploited, and as a consequence, one is often led to focus on the measurement of surface impedance variations $\Delta Z_s = Z_s(x) - Z_s(x_r)$ induced by an external parameter x (e.g., the temperature T or the magnetic field H), whose reference value is denoted x_r. Absolute quantities, instead of variations only, can, thus, be recovered if the reference value $Z_s(x_r)$ can be evaluated with other means (e.g., by using the Hagens–Rubens $R_s = X_s$ condition in metals with real ρ or by taking $Z_s(T \ll T_c) \sim 0$ in superconductors). It is worth mentioning that the real and imaginary parts of ΔZ_s mainly depend on the modulus and the phase of Γ_m, respectively [28]. Since the phase of Γ_m is very sensitive to small temperature changes of the properties of the line, when long thermalizations to attain high enough T stability are not feasible, the accuracy of ΔX_s is worse than the one on ΔR_s. In the approximated calibration scheme proposed in [28], [57]

$$\Delta Z_s = Z_s(x) - Z_s(x_r) \approx Z_l \frac{1 - \frac{\Gamma(x)}{\Gamma(x_r)}}{1 + \frac{\Gamma(x)}{\Gamma(x_r)}}, \frac{\Gamma(x)}{\Gamma(x_r)} \approx \frac{\tilde{\Gamma}(x)}{\tilde{\Gamma}(x_r)} \frac{\tilde{\alpha}(x_r)}{\tilde{\alpha}(x)} \tag{30}$$

where $\tilde{\Gamma}$ denotes the reflection coefficient obtained from $\Gamma_m(T)$ by inverting (29) with S_{ij}^{line} at room temperature T_{room} (which would yield a correct Γ only for $T = T_{\text{room}}$); $\tilde{\alpha}$ represents the residual contribution of the measurement line ($\tilde{\alpha} = 1$ in the ideal case $T = T_{\text{room}}$); and the "≈" signs indicate that negligible contributions with respect to the dominant uncertainty terms reported below have been discarded. Thus, $u(\Delta Z_s)$ arises from $u(\tilde{\Gamma})$, $u(\tilde{\Gamma}(x_r))$, $u(\tilde{\alpha}(x_r)/\tilde{\alpha}(x))$, and $u(Z_l)$. The influence of $u(Z_l)$ can be avoided by working with normalized quantities; $u(\tilde{\Gamma})$ and $u(\tilde{\Gamma}_r)$, of the order of 0.01, can be evaluated from (29), where $u(\Gamma_m)$ and $u(S_{ij}^{\text{line}})$ are obtained from the VNA datasheet [28]; and $u(\tilde{\alpha}(x_r)/\tilde{\alpha}(x))$ is evaluated in [28] providing a relative uncertainty of the order of 1%. Hence, $u(\Delta Z_s) \sim 1\,\Omega$ when $Z_s \sim 100\,\Omega$ and neglecting $u(Z_l)$.

B. Electromagnetic Resonators

In resonators, e.m. field (quasi)stationary spatial configurations (*resonant modes*) can be excited at proper resonant frequencies. In the *surface* perturbative approach, the sample to be measured constitutes one of the limiting conducting surfaces [see Fig. 8(b)] and contributes to the overall resonator power dissipation P and (time-averaged) reactive energy storage W_{em} through its R_s and X_s, respectively. For a given mode with resonating frequency ν_0 and unloaded quality factor $Q = 2\pi\nu_0 W_{\text{em}}/P$, the sample R_s and *variations* of X_s can be obtained as follows [16], [50], [58]:

$$R_s + \mathrm{i}\Delta X_s = G_s \left(\frac{1}{Q} - \mathrm{i}2\frac{\Delta\nu_0}{\nu_0} \right) - \text{background} \tag{31}$$

where the variations are with respect to a reference value; "background" represents the contributions to Q and $\Delta\nu_0$ by the resonator structure, sample excluded; and G_s is a geometrical factor that depends on the resonant mode and can be either measured with known samples or, more often, computed analytically or through e.m. simulations. Once coupled to a microwave line with two ports, the frequency-dependent transmission coefficient S_{21} of the resonator is ideally

$$S_{21}(\nu) = \frac{S_{21}(\nu_0)}{1 + 2\mathrm{i}Q_l(\nu/\nu_0 - 1)} \tag{32}$$

where the loaded quality factor $Q_l = \beta Q$, with the coupling factor $0 < \beta \ll 1$ for small couplings. $|S_{21}(\nu)|^2$ is a Lorentzian bell-shaped curve with center frequency ν_0 and full-width at half-maximum $\Delta\nu_{\text{FWHM}} = \nu_0/Q_l$. Performing a frequency sweep around ν_0, the measured $S_{21}(\nu)$ can be fit to extract Q_l and ν_0, and the Q is obtained once β is determined

[5]Equation (28) is written here in terms of wave impedances instead of characteristic impedance [15]. In the latter case, Z_l is commonly $50\,\Omega$ or $75\,\Omega$, and the impedance extracted from (28) must be corrected by a geometrical factor taking into account the radii of the coaxial cable.

from the reflection coefficients S_{11} and S_{22}. Concerning the accuracy of the measured $R_s + \mathrm{i}\Delta X_s$, (31) yields [50]

$$u^2(R_s) = \left(\frac{G_s}{Q}\right)^2 \left[\left(\frac{u(Q)}{Q}\right)^2 + \left(\frac{u(G_s)}{G_s}\right)^2\right] \quad \text{(33a)}$$

$$u^2(\Delta X_s) = \left[2\left(\frac{2G_s}{\nu_0}\right)^2 \left(\frac{u(\nu_0)}{\nu_0}\right)^2 + (\Delta X_s)^2 \left(\frac{u(G_s)}{G_s}\right)^2\right]. \quad \text{(33b)}$$

It is apparent that high Q is desirable for high accuracy on R_s. As a rough example, taking $G_s \sim 10^3$ and $Q \sim 10^4$ with a typical $u(Q) \sim 10 - 100$ ($u(Q)/Q < 1\%$), one obtains $u(R_s) \sim 1\,\mathrm{m}\Omega$, three orders of magnitude lower than the value for the Corbino disk technique. Here, many issues have been neglected, including the resonator background contribution and the use of uncalibrated microwave lines, unavoidable in cryogenic environments, which can yield $u(Q)/Q$ up to 2% [50], [59], [60]. In addition, similar to what happens for the Corbino technique, accuracy on ΔX_s can be worse than the one on ΔR_s when temperature variations are involved, for example, in T-ranges where the dielectric ε_r varies significantly.

High Q is needed also for small $u(\Delta X_s)$ even though Q does not explicitly appear in it, as it can be qualitatively[6] understood considering that the width of the Lorentzian curve, whose center yields ν_0, is $\propto Q^{-1}$.

VII. Experimental Section

In this section, we provide some examples of actual measurements of surface impedance performed on distinct samples, each belonging to a different regime for the general expression for Z_s reported in (6). The goal is twofold, both to show real situations in which the various alternative regimes and subsequent applicable simplified models apply and to provide study cases of uncertainty evaluation.

A. Bulk Limit Regime

We consider a surface resistance measurement performed on a bulk Nb_3Sn sample at T near its critical temperature T_c, with no applied magnetic field [61], [62], with a resonator with $\nu_0 \simeq 14.9\,\mathrm{GHz}$. Measurement results are reported in Fig. 9, where error bars represent the standard uncertainty, which is mainly affected by a systematic contribution due to the uncalibrated cryogenic microwave line [50], [59], [60].

Starting from R_s and assuming the normal state (i.e., at $T > T_c$) resistivity ρ_n purely real, by means of the bulk expression (4), one can compute $\rho_n = R_s^2/(\pi\nu\mu_0)$ with $\nu = \nu_0$. The uncertainty $u(\rho_n)$ can be easily evaluated

$$\left(\frac{u(\rho_n)}{\rho_n}\right)^2 = 4\left(\frac{u(R_s)}{R_s}\right)^2 + \left(\frac{u(\nu_0)}{\nu_0}\right)^2 + \left(\frac{u(\mu_0)}{\mu_0}\right)^2 \quad (34)$$

where $u(\nu_0)/\nu_0 \sim 10^{-6}$ and $u(\mu_0)/\mu_0 = 1.5 \times 10^{-10}$ [17] can be safely neglected. The obtained $\rho_n = 14.7(15)\,\mu\Omega\,\mathrm{cm}$

[6]For example, a noise level given by a fraction h_n of $S_{21}(\nu_0)$ would mask the true maximum position within a ν range $\propto Q^{-1}$, yielding $u(\nu_0)/\nu_0 = (h_n/2)^{1/2}/Q$.

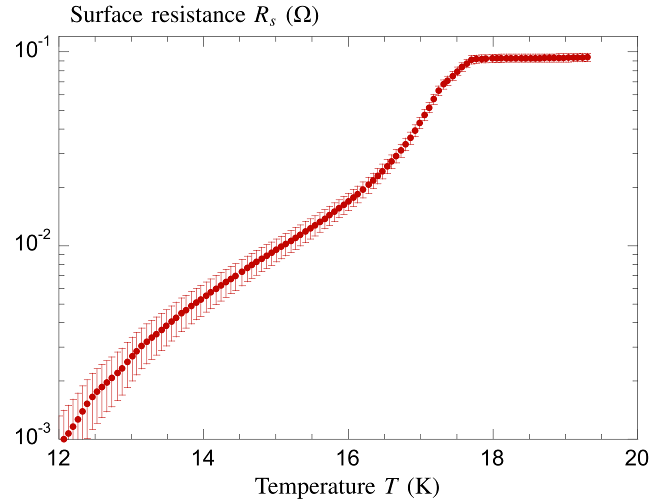

Fig. 9. Surface resistance versus T on a bulk Nb_3Sn sample at 14.9 GHz.

near T_c is in agreement with the literature [63], [64] and, thus, is consistent with the bulk limit regime.

B. Thin Film Regime

We provide here a measurement example in which the thin film regime applies, showing a standard data analysis with the evaluation of the uncertainties. Resistivity values are extracted with both the full model (6) and the simplified one (21) and compared, and the conditions for the applicability of the thin film expressions are analyzed. To validate this regime in a compelling way, the $Z_s \propto t_s^{-1}$ dependence could be explored among a set of thin films with different t_s, but the often observed thickness-dependent conductivity [65] makes this path not viable. Thus, we study instead a material with a pronounced frequency-dependent $\rho(\nu)$: an observed $Z_s(\nu) \propto \rho(\nu)$ would validate the thin film regime. To this aim, we exploit type II superconductors in a magnetic field. In this case, the frequency dependence of ρ is [22]

$$\rho(\nu) = \rho_{\mathrm{sat}} \frac{1}{1 - \mathrm{i}\nu_c/\nu} \quad (35)$$

where ν_c is a characteristic frequency and ρ_{sat} a scale factor. The measurement of a ν-dependent Z_s benefits from the wideband nature of the Corbino disk technique. The latter is, therefore, used for measurements on Nb [57], [66], [67], a well-known conventional superconductor, in the form of a thin film with $t_s = 40(4)\,\mathrm{nm}$ and $T_c = 6.4(1)\,\mathrm{K}$, grown on an Al_2O_3 substrate $0.50(3)\,\mathrm{mm}$ thick [35]. A static magnetic field $\mu_0 H = 0.80\,\mathrm{T}$ is applied normally to the film surface.

A preliminary quick check about the applicability conditions can be straightforwardly done. The d.c. measurements yield $\rho_n = 13(1)\,\mu\Omega\,\mathrm{cm}$ (which sets the scale for $\rho_{\mathrm{sat}} \leq \rho_n$) and, thus, the normal state skin depth $\delta_n = 1.8\,\mu\mathrm{m}$ at $\nu = 10\,\mathrm{GHz}$, while $\lambda = 160\,\mathrm{nm}$ [68]: once compared with the thickness t_s, condition (18) holds. The sapphire substrate ($\varepsilon_r = 9.27(1)$ [33]) yields $Z_d \simeq 124\,\Omega$, which sets the scale for $Z_{s[\mathrm{sub}]}$, much larger than $R_n \simeq 3.2\,\Omega$ (the resistance exhibited in the normal state, estimated as $R_n \simeq \rho_n/t_s$), which sets the scale for Z_{sf}: hence, conditions (20a) and (20b) are expected to be verified.

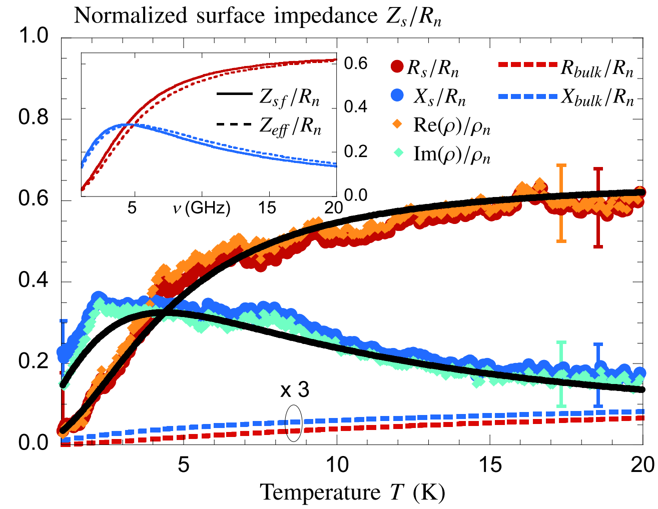

Fig. 10. Full dots: normalized surface impedance versus frequency, at fixed $T = 4.5\,\mathrm{K}$ and field $H = 0.8\,\mathrm{T}$, for an Nb thin film, measured with a Corbino disk setup; error bars represent standard uncertainty; diamonds: normalized ρ extracted through Z_{eff} expression; continuous black lines: fits experimental data; and dashed lines: equivalent (see text) bulk surface impedance. Inset: comparison between numerically computed Z_{sf} and Z_{eff}.

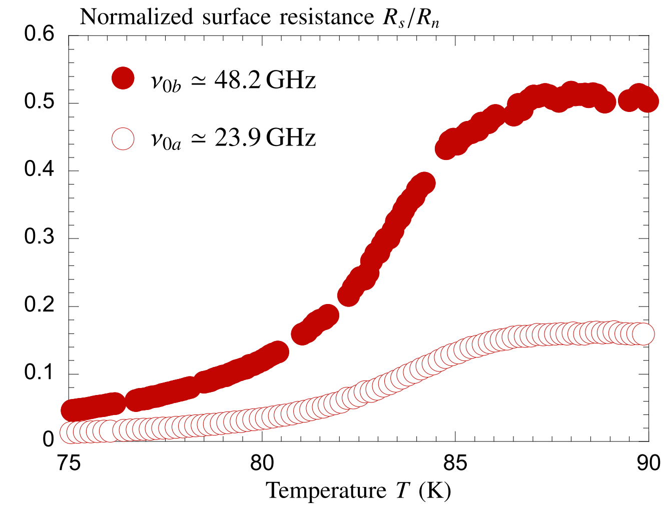

Fig. 11. Measurement of the surface resistance versus T for a YBCO thin film over Silicon substrate at two frequencies (error bars are within dot size).

In Fig. 10, the real and imaginary parts of the measured Z_s at $T = 4.5\,\mathrm{K}$ are reported, normalized to the normal state resistance $R_n = \mathrm{Re}(Z_s(H^*))$ (driving the superconductor in the normal state by the application of a sufficiently high static magnetic field $\mu_0 H = 1.8T$). The reported Z_s is computed from (30), using as a reference a combination of the zero field $Z_s(H = 0)$ (whose real part is negligible in a superconductor) and normal state $Z_s(H^*)$ [28], [57]. The uncertainty, reported as error bars, is computed, as discussed in Section VI-A and [28].

Then, we work within the thin film regime, $Z_s(\nu) = \rho(\nu)/t_s$ (which yields a real $Z_s(H^*) = R_n = \rho_n/t_s$ in the normal state), to check if a fit can be performed through (35). The fit yields $\nu_c = 4.4(1)\,\mathrm{GHz}$, which dictates the frequency-dependent part, and $\rho_{\mathrm{sat}}/\rho_n = 0.65(1)$. The obtained fit is reported as continuous black lines in Fig. 10. The uncertainties on the fit parameters have been computed by the fitting Levenberg–Marquardt algorithm [69] receiving in input the uncertainty on Z_s/R_n. As it can be seen, the frequency dependence is very well captured, thus validating the thin film regime.

For comparison, the same measured data are analyzed within the full expression (6), which is numerically solved to extract $\rho_{Z_{\mathrm{eff}}}$. To compute also the uncertainty, the numerical solution of (6) is obtained with Monte Carlo runs, taking into account all the uncertainties on the measured Z_s and all the additionally needed parameters (ρ_n, t_s, t_d, ε_r, and ρ_m), so that the normalized $\rho_{Z_{\mathrm{eff}}}/\rho_n$ and its uncertainty are computed as means and standard deviations on the runs, respectively. The results are reported in Fig. 10 as diamonds. A significant result of this analysis is that both the normalized resistivity and its uncertainty remain identical in the thin film regime, regardless of whether they are calculated using the full model Z_{eff} or the simplified model Z_{sf}. It is, thus, confirmed the feasibility, with all its advantages, of the use of the simplified model.

As an additional check, in Fig. 10, the bulk impedance computed with the fit ρ, i.e., the impedance that Nb would exhibit if it were infinitely thick but with the same resistivity, is reported as dashed lines. It can be seen that the resulting ν dependence is totally different from the measured one, which, instead, is correctly described by the thin film model.

As a final check, the fit ρ can be used to numerically compute Z_{eff} [see (6)] (using the nominal values for the substrate properties) to be compared with the computed $Z_{\mathrm{sf}} = \rho/t_s$. The result, reported in the inset of Fig. 10, shows that Z_{sf} is indistinguishable from Z_{eff} within the error bars (reported only in the main figure). Hence, it is confirmed that $\Delta\rho_a \simeq \Delta Z_{a\%}$, enabling the use of the latter for a computational fast a posteriori check on the thin film regime.

C. Substrate Effect Regime

In this section, we provide an example of a surface impedance measured on a thin film (i.e., having thickness t_s much smaller than the e.m. field penetration depth) in which the substrate effect is, nevertheless, not negligible, i.e., the condition $|Z_{s[\mathrm{sub}]}| \gg |Z_{\mathrm{sf}}|$ does not hold. A pertinent study case is given by an YBCO film, $80\,\mathrm{nm}$ thick, grown over a Si substrate $\sim 300\,\mathrm{nm}$ thick. With the help of two metal cavities, operating at $\nu_{0a} \simeq 23.9\,\mathrm{GHz}$ and $\nu_{0b} \simeq 48.2\,\mathrm{GHz}$, the sample Z_s is measured near T_c [38], [70]. In Fig. 11, the normalized $R(T)/R_n$ is reported for both frequencies, with $R_n = \rho_{dc}(T \gtrsim T_c)/t_s$ being the normal state resistance that the sample would have in the thin film limit. As it can be seen, the resistances are neither equal in the normal state, as it would happen in the thin film regime, nor scale as $(\nu_{0b}/\nu_{0a})^{1/2} = 1.42$, as it would happen in the bulk limit. By using the full expression for Z_{eff} and by properly determining the substrate impedance, it is possible to reconcile these results. We do not report the remainder of the analysis, already performed and available in [38] and [70], since, in Section VII-D, we provide an even more “dramatic” example of substrate effect, but we remark here the importance that substrate effects can have in technologically relevant structures.

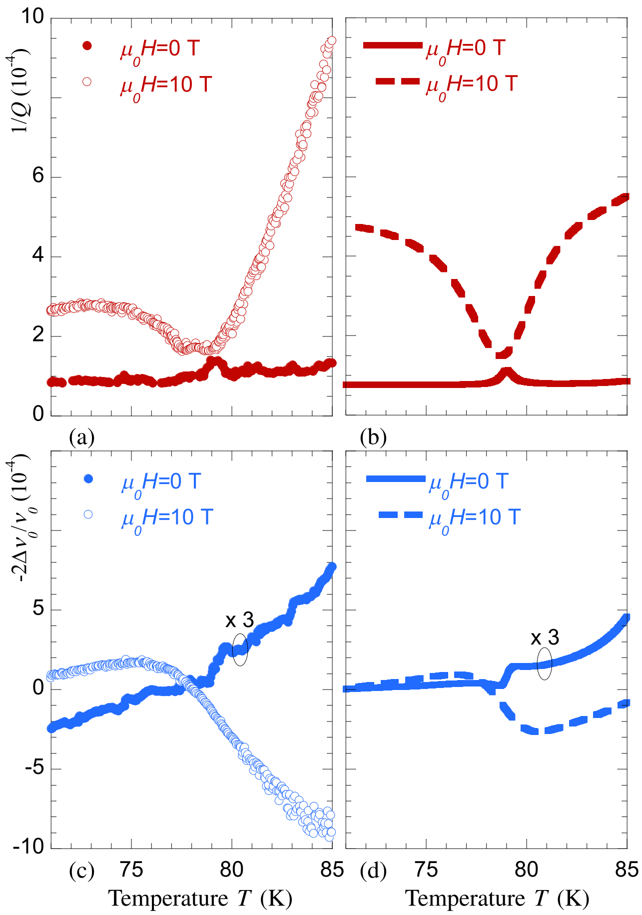

Fig. 12. (a) and (c) Measured Z_s versus T near a substrate resonance in a $YBa_2Cu_3O_{7-\delta}$ thin film grown on a $SrTiO_3$ substrate. In the absence of an applied magnetic field, an upward peak appears in R_s, accompanied by an upward step in X_s. With an increased $\mathrm{Re}(\rho)$ induced by a strong magnetic field $\mu_0 H = 10\,\mathrm{T}$, the peak becomes a valley, and the upward step transforms into a downward step. Error bars are within dot size. (b) and (d) Corresponding numerical simulations of Z_s (parameters reported in the text). The calculations reproduce the experimentally observed features.

D. Substrate Resonance Regime

In this section, we provide an experimental example of the effects predicted by the calculations in Section V-B. We choose a thin superconducting $YBa_2Cu_3O_{7-\delta}$ film, $100\,\mathrm{nm}$ thick, grown over a ferroelectric $SrTiO_3$ substrate. In order to place the system near a substrate resonance but with a mainly reactive thin film, we set $T < T_c$. We then tune the permittivity of the substrate by changing T [37], thus measuring the change in R_s and X_s around the substrate resonance. We expect to observe a peak in R_s at the substrate resonance. We then apply a strong magnetic field: hence, an additional contribution, predominantly resistive in the (10–20)-GHz range [43], [71], enters the resistivity. In this way, we move the thin film toward a more resistive behavior while keeping unchanged the substrate parameters. We then expect to observe a crossover between the mentioned peak and a dip (or valley) in R_s when the external field is applied. The surface reactance should behave consistently and in agreement with the numerical results. We should remark that the field-induced contribution is strongly T-dependent, with complicated and still debated dependences. Thus, the fine details are beyond a quantitative analysis.

Measurements were performed at $14.9\,\mathrm{GHz}$ through a dielectric-loaded cylindrical resonator used with the surface perturbation method, briefly recalled in Section VI-B and extensively described elsewhere [58]. The main differences here are the frequency and the nontrivial capability of operation in very high magnetic fields. In Fig. 12(a) and (c), measurements performed by varying T at two selected field values ($\mu_0 H = 0\,\mathrm{T}$ and $10\,\mathrm{T}$) are reported in term of $1/Q \propto R_s$ and $-2\Delta\nu_0/\nu_0 \propto \Delta X_s$ (raw data, without background subtraction are shown). An anomaly is apparent around $79\,\mathrm{K}$, with the expected behavior: it appears in R_s as an upward peak for $\mu_0 H = 0\,\mathrm{T}$ (mostly reactive film) and a downward valley for $\mu_0 H = 10\,\mathrm{T}$ (significant resistive contribution). Consistently, an upward step (with increasing T) appears in ΔX_s in zero field, which becomes a downward step for $\mu_0 H = 10\,\mathrm{T}$. The peak/step structure, its evolution, and the different amplitudes with and without the resistive contribution added to the overall resistivity can be quite well reproduced by using (6) and (9), the two-fluid model of (27) with the YBCO parameters reported with $T_c = 88\,\mathrm{K}$, $\varepsilon_r(T)$ as reported previously [37], and a small T-independent real additive background $\sim 7.7 \times 10^{-5}$. The calculated results are reported in Fig. 12(b) and (d), as $1/Q$ and $-2\Delta\nu_0/\nu_0$ for homogeneity with the experimental data. Thus, it is confirmed that a resistive/reactive film exhibits downward/upward substrate resonances in R_s.

VIII. Conclusion

In this article, we have explored the problem of the extraction of microwave complex resistivity from surface impedance measurements on thin conducting and superconducting films. We took into account the commonly used simplified models for the thin film regime illustrating the analytical conditions for their applicability, discussing the role of the sample geometry and e.m. properties in determining the measurement uncertainties, and comparing these uncertainties with the quantification provided by the analytical conditions themselves. In particular, we have shown that the use of simplified models finds, in general, a set of ranges of frequency and film thickness where the approximation error, is below 1%, with respect to the use of the full expression. This holds true also in the potentially critical case of superconducting films, where the conductivity is mainly imaginary. We have compared these values with the uncertainties arising from the measurement itself, typically $\sim 1\%$ and up to $\sim 10\%$ within cryogenic environments, due to their specific issues related to the calibration of the microwave line.

We have then extensively validated the models by presenting several examples of real measurements, chosen as application cases for the various discussed regimes for the surface impedance. In particular, we have reported compelling examples where the thin film model, with its simplicity, accurately describes the experimental findings, providing a throughout data analysis in which the full and simplified models have been compared both in terms of the measurand and its uncertainty.

ACKNOWLEDGMENT

The authors thank G. Celentano of the ENEA Research Center, Frascati, Italy, and C. Attanasio of the Universitã degli Studi di Salerno, Italy, for the $YBa_2Cu_3O_{7-\delta}$ and Nb films, respectively.

REFERENCES

[1] D. E. Steinhauer, C. P. Vlahacos, S. K. Dutta, B. J. Feenstra, F. C. Wellstood, and S. M. Anlage, "Quantitative imaging of sheet resistance with a scanning near-field microwave microscope," *Appl. Phys. Lett.*, vol. 72, no. 7, pp. 861–863, Feb. 1998.

[2] J. Krupka and J. Mazierska, "Contactless measurements of resistivity of semiconductor wafers employing single-post and split-post dielectric-resonator techniques," *IEEE Trans. Instrum. Meas.*, vol. 56, no. 5, pp. 1839–1844, Oct. 2007.

[3] Y. Kobayashi and H. Yoshikawa, "Microwave measurements of surface impedance of high-T_c superconductors using two modes in a dielectric rod resonator," *IEEE Trans. Microw. Theory Techn.*, vol. 46, no. 12, pp. 2524–2530, Dec. 1998.

[4] S. Calatroni, "HTS coatings for impedance reduction in particle accelerators: Case study for the FCC at CERN," *IEEE Trans. Appl. Supercond.*, vol. 26, no. 3, pp. 1–4, Apr. 2016.

[5] A. Alimenti, N. Pompeo, K. Torokhtii, and E. Silva, "Surface impedance measurements in superconductors in DC magnetic fields: Challenges and relevance to particle physics experiments," *IEEE Instrum. Meas. Mag.*, vol. 24, no. 9, pp. 12–20, Dec. 2021.

[6] A. Alimenti, K. Torokhtii, D. Di Gioacchino, C. Gatti, E. Silva, and N. Pompeo, "Impact of superconductors' properties on the measurement sensitivity of resonant-based axion detectors," *Instruments*, vol. 6, no. 1, p. 1, Dec. 2021.

[7] M. L. Stutzman, M. Lee, and R. F. Bradley, "Broadband calibration of long lossy microwave transmission lines at cryogenic temperatures using nichrome films," *Rev. Sci. Instrum.*, vol. 71, no. 12, pp. 4596–4599, Dec. 2000.

[8] S. Sridhar, "Microwave response of thin-film superconductors," *J. Appl. Phys.*, vol. 63, no. 1, pp. 159–166, Jan. 1988.

[9] P. Hartemann, "Effective and intrinsic surface impedances of high-T_c superconducting thin films," *IEEE Trans. Appl. Supercond.*, vol. 2, no. 4, pp. 228–235, Dec. 1992.

[10] E. Silva, M. Lanucara, and R. Marcon, "The effective surface resistance of superconductor/dielectric/metal structures," *Superconductor Sci. Technol.*, vol. 9, no. 11, pp. 934–941, Nov. 1996.

[11] N. Pompeo, K. Torokhtii, and E. Silva, "Surface impedance measurements in thin conducting films: Substrate and finite-thickness-induced uncertainties," in *Proc. IEEE Int. Instrum. Meas. Technol. Conf. (I2MTC)*, May 2017, pp. 1–5.

[12] *International Standard Intrinsic Surface Impedance of Superconductors*, document IEC 61788-15, International Electrotechnical Commission, 2011.

[13] L. D. Landau and E. M. Lifshifts, *Physical Kinetics*, 1st ed., New York, NY, USA: Pergamon Press, 1981.

[14] J. D. Jackson, *Classical Electrodynamics*, 3rd ed., Hoboken, NJ, USA: Wiley, 1999.

[15] D. M. Pozar, *Microwave Engineering*, 4th ed., Hoboken, NJ, USA: Wiley, 2011.

[16] R. E. Collin, *Foundation for Microwave Engineering*, 2nd ed., Singapore: McGraw-Hill, 1992.

[17] *CODATA Internationally Recommended 2018 Values of the Fundamental Physical Constants*. Accessed: Feb. 22, 2022. [Online]. Available: https://physics.nist.gov/cuu/Constants/index.html

[18] K. Zhang, *Electromagnetic Theory for Microwaves and Optoelectronics*. Berlin, Germany: Springer, 2008.

[19] L. D. Landau and E. M. Lifshifts, *Electrodynamics of Continuous Media* (Course of Theoretical Physics), vol. 8, 2nd ed., Amsterdam, The Netherlands: Pergamon, 1984.

[20] T. S. Saad, *Microwave Engineers' Handbook*, vol. 2. Norwood, MA, USA: Artech House, 1971.

[21] N. W. Ashcroft and N. D. Mermin, *Solid State Physics*. San Diego, CA, USA: Harcour College Publishers, 1976.

[22] M. Tinkham, *Introduction to Superconductivity*, 2nd ed., New York, NY, USA: McGraw-Hill, 1996.

[23] N. Pompeo, A. Alimenti, K. Torokhtii, and E. Silva, "Physics of vortex motion by means of microwave surface impedance measurements (review article)," *Low Temp. Phys.*, vol. 46, no. 4, pp. 343–347, Apr. 2020.

[24] T. P. Orlando and K. A. Delin, *Foundations of Applied Superconductivity*. Reading, MA, USA: Addison-Wesley, 1990.

[25] M. W. Coffey and J. R. Clem, "Unified theory of effects of vortex pinning and flux creep upon the RF surface impedance of type-II superconductors," *Phys. Rev. Lett.*, vol. 67, no. 3, pp. 386–389, Jul. 1991.

[26] D. Kajfez and P. Guillon, *Dielectric Resonators*, 2nd ed. GA, USA: Noble Publishing Corporation, 1986.

[27] J. H. Lee et al., "Accurate measurements of the intrinsic surface impedance of thin $YBa_2Cu_3O_7 - \delta$ films using a modified two-tone resonator method," *IEEE Trans. Appl. Supercond.*, vol. 15, no. 2, pp. 3700–3705, Jun. 2005.

[28] E. Silva, N. Pompeo, K. Torokhtii, and S. Sarti, "Wideband surface impedance measurements in superconducting films," *IEEE Trans. Instrum. Meas.*, vol. 65, no. 5, pp. 1120–1129, May 2016.

[29] R. A. Matula, "Electrical resistivity of copper, gold, palladium, and silver," *J. Phys. Chem. Reference Data*, vol. 8, no. 4, pp. 1147–1298, Oct. 1979.

[30] R. A. Serway, *Principles of Physics*. New York, NY, USA: Saunders College Pub, 1998.

[31] N. Pompeo, K. Torokhtii, A. Alimenti, A. Mancini, G. Celentano, and E. Silva, "Vortex pinning and flux flow microwave studies of coated conductors," *IEEE Trans. Appl. Supercond.*, vol. 29, no. 5, pp. 1–5, Aug. 2019.

[32] G. Hartwig, *Polymer Properties At Room and Cryogenic Temperatures*. New York, NY, USA: Plenum Press, 1994.

[33] J. Krupka, K. Derzakowski, M. Tobar, J. Hartnett, and R. G. Geyer, "Complex permittivity of some ultralow loss dielectric crystals at cryogenic temperatures," *Meas. Sci. Technol.*, vol. 10, no. 5, pp. 387–392, May 1999.

[34] J. Krupka, R. G. Geyer, M. Kuhn, and J. H. Hinken, "Dielectric properties of single crystals of Al_2O_3, $LaAlO_3$, $NdGaO_3$, $SrTiO_3$, and MgO at cryogenic temperatures," *IEEE Trans. Microw. Theory Techn.*, vol. 42, no. 10, pp. 1886–1890, Jun. 1994.

[35] *Kyocera Single-Crystal Sapphire Products*. Accessed: Jan. 26, 2022. [Online]. Available: https://global.kyocera.com/prdct/fc/list/category/sapphire/index.html

[36] M. M. Felger, M. Dressel, and M. Scheffler, "Microwave resonances in dielectric samples probed in Corbino geometry: Simulation and experiment," *Rev. Sci. Instrum.*, vol. 84, no. 11, Nov. 2013, Art. no. 114703.

[37] N. Pompeo, L. Muzzi, V. Galluzzi, R. Marcon, and E. Silva, "Measurements and removal of substrate effects on the microwave surface impedance of YBCO films on $SrTiO_3$," *Superconductor Sci. Technol.*, vol. 20, no. 10, pp. 1002–1008, Oct. 2007.

[38] N. Pompeo, R. Marcon, L. Méchin, and E. Silva, "Effective surface impedance of $YBa_2Cu_3O_{7-\delta}$ films on silicon substrates," *Superconductor Sci. Technol.*, vol. 18, no. 4, pp. 531–537, Apr. 2005.

[39] B. D. Hall, "On the propagation of uncertainty in complex-valued quantities," *Metrologia*, vol. 41, no. 3, pp. 173–177, Jun. 2004.

[40] *Evaluation of Measurement Data—Supplement 2 to the Guide to the Expression of Uncertainty in Measurement—Extension to Any Number of Output Quantities*, document JCGM 102:2011, Joint Committee for Guides in Metrology, 2011.

[41] N. Klein et al., "The effective microwave surface impedance of high-T_c thin films," *J. Appl. Phys.*, vol. 67, no. June, pp. 6940–6945, 1990.

[42] *Guide to the Expression of Uncertainty in Measurement—Part 6: Developing and Using Measurement Models*, document JCGM GUM-6:2020, Joint Committee for Guides in Metrology, 2020.

[43] C. Poole, *Superconductivity*, 2nd ed., Amsterdam, The Netherlands: Academic, 2007.

[44] A. Frolova et al., "Analysis of transport properties of MOD YBCO films with $BaZrO_3$ as artificial vortex pinning centers," *IEEE Trans. Appl. Supercond.*, vol. 26, no. 3, pp. 1–5, Apr. 2016.

[45] L. F. Chen, C. K. Ong, C. P. Neo, V. V. Varadan, and V. K. Varadan, *Microwave Electronics: Measurement and Materials Characterization*. Hoboken, NJ, USA: Wiley, 2004.

[46] J. C. Booth, D. H. Wu, and S. M. Anlage, "A broadband method for the measurement of the surface impedance of thin films at microwave frequencies," *Rev. Sci. Instrum.*, vol. 65, no. 6, pp. 2082–2090, Jun. 1994.

[47] H. Kitano, T. Ohashi, and A. Maeda, "Broadband method for precise microwave spectroscopy of superconducting thin films near the critical temperature," *Rev. Sci. Instrum.*, vol. 79, no. 7, Jul. 2008, Art. no. 074701.

[48] M. V. Jacob, J. Mazierska, D. Ledenyov, and J. Krupka, "Microwave characterisation of CaF_2 at cryogenic temperatures using a dielectric resonator technique," *J. Eur. Ceram. Soc.*, vol. 23, no. 14, pp. 2617–2622, Jan. 2003.

[49] N. T. Cherpak, A. A. Barannik, S. A. Bunyaev, Y. V. Prokopenko, and S. A. Vitusevich, "Measurements of millimeter-wave surface resistance and temperature dependence of reactance of thin HTS films using quasi-optical dielectric resonator," *IEEE Trans. Appl. Supercond.*, vol. 15, no. 2, pp. 2919–2922, Jun. 2005.

[50] A. Alimenti, K. Torokhtii, E. Silva, and N. Pompeo, "Challenging microwave resonant measurement techniques for conducting material characterization," *Meas. Sci. Technol.*, vol. 30, no. 6, Jun. 2019, Art. no. 065601.

[51] D. Kajfez, "A-posteriori estimation of random uncertainty for the reflection type Q-factor measurements," *Appl. Comput. Electromagn. Soc.*, vol. 35, no. 10, pp. 1105–1112, Dec. 2020.

[52] J. Powell, A. Porch, R. Humphreys, F. Wellhöfer, M. Lancaster, and C. Gough, "Field, temperature, and frequency dependence of the surface impedance of $YBa_2Cu_3O_7$ thin films," *Phys. Rev. B, Condens. Matter*, vol. 57, no. 9, pp. 5474–5484, Mar. 1998.

[53] T. Hashimoto and Y. Kobayashi, "An image-type dielectric resonator method to measure surface resistance of a high-T_c superconductor film," *IEICE Trans. Electron.*, vols. E86-C, no. 1, pp. 30–36, 2003.

[54] N. Pompeo, K. Torokhtii, A. Alimenti, G. Sylva, V. Braccini, and E. Silva, "Pinning properties of FeSeTe thin film through multifrequency measurements of the surface impedance," *Superconductor Sci. Technol.*, vol. 33, no. 11, Nov. 2020, Art. no. 114006.

[55] N. Pompeo, K. Torokhtii, A. Alimenti, and E. Silva, "A method based on a dual frequency resonator to estimate physical parameters of superconductors from surface impedance measurements in a magnetic field," *Measurement*, vol. 184, Nov. 2021, Art. no. 109937.

[56] M. Scheffler and M. Dressel, "Broadband microwave spectroscopy in Corbino geometry for temperatures down to 1.7 k," *Rev. Sci. Instrum.*, vol. 76, no. 7, Jul. 2005, Art. no. 074702.

[57] E. Silva, N. Pompeo, and S. Sarti, "Wideband microwave measurements in $Nb/Pd_{84}Ni_{16}/Nb$ structures and comparison with thin Nb films," *Superconductor Sci. Technol.*, vol. 24, no. 2, Feb. 2011, Art. no. 024018.

[58] N. Pompeo, K. Torokhtii, and E. Silva, "Dielectric resonators for the measurements of the surface impedance of superconducting films," *Meas. Sci. Rev.*, vol. 14, no. 3, pp. 164–170, Jun. 2014.

[59] K. Torokhtii et al., "Q-factor of microwave resonators: Calibrated vs. uncalibrated measurements," *J. Phys., Conf. Ser.*, vol. 1065, Aug. 2018, Art. no. 052027.

[60] K. Torokhtii, A. Alimenti, N. Pompeo, and E. Silva, "Estimation of microwave resonant measurements uncertainty from uncalibrated data," *ACTA IMEKO*, vol. 9, no. 3, p. 47, Sep. 2020.

[61] A. Alimenti, N. Pompeo, K. Torokhtii, T. Spina, L. Muzzi, and E. Silva, "Surface impedance measurements on Nb_3Sn in high magnetic fields," *IEEE Trans. Appl. Supercond.*, vol. 29, no. 5, Aug. 2019, Art. no. 3500104.

[62] A. Alimenti et al., "Microwave measurements of the high magnetic field vortex motion pinning parameters in Nb_3Sn," *Superconductor Sci. Technol.*, vol. 34, no. 1, Jan. 2021, Art. no. 014003.

[63] R. Flükiger, H. Küpfer, J. Jorda, and J. Müller, "Effect of atomic ordering and composition changes on the electrical resistivity of Nb_3Al, Nb_3Sn, Nb_3Ge, Nb_3Ir, V_3Si and V_3Ga," *IEEE Trans. Magn.*, vol. MTT-23, no. 2, pp. 980–983, Jan. 1987.

[64] A. Godeke, "Properties of Nb_3Sn and their variation with A15 composition, morphology and strain state," *ChemInform*, vol. 37, no. 43, pp. R68–R80, Oct. 2006.

[65] D. Janjušević et al., "Microwave response of thin niobium films under perpendicular static magnetic fields," *Phys. Rev. B, Condens. Matter*, vol. 74, no. 10, Sep. 2006, Art. no. 104501.

[66] N. Pompeo, K. Torokhtii, and E. Silva, "Superfluid density and vortex dynamics in S/F/S heterostructures," *J. Supercond. Novel Magnetism*, vol. 28, no. 3, pp. 1097–1101, Aug. 2014.

[67] R. Loria et al., "Robustness of the 0-π transition against compositional and structural ageing in superconductor/ferromagnetic/superconductor heterostructures," *Phys. Rev. B, Condens. Matter*, vol. 92, no. 18, Nov. 2015, Art. no. 184106.

[68] A. I. Gubin, K. S. Il'in, S. A. Vitusevich, M. Siegel, and N. Klein, "Dependence of magnetic penetration depth on the thickness of superconducting nb thin films," *Phys. Rev. B, Condens. Matter*, vol. 72, no. 6, Aug. 2005, Art. no. 064503.

[69] M. Žic, "An alternative approach to solve complex nonlinear least-squares problems," *J. Electroanal. Chem.*, vol. 760, pp. 85–96, Jan. 2016.

[70] N. Pompeo, R. Marcon, and E. Silva, "Substrate contribution to the surface impedance of HTS films on Si," *J. Supercond. Novel Magnetism*, vol. 19, nos. 7–8, pp. 611–615, Jan. 2007.

[71] N. Pompeo and E. Silva, "Reliable determination of vortex parameters from measurements of the microwave complex resistivity," *Phys. Rev. B, Condens. Matter*, vol. 78, no. 9, Sep. 2008, Art. no. 094503.

Open Access funding provided by 'Università degli Studi Roma Tre' within the CRUI CARE Agreement